Proceedings of the 17th World Congress
The International Federation of Automatic Control
Seoul, Korea, July 6-11, 2008

Disturbances Rejection for Precise Position Control of Linear Switched Reluctance Motors

Shi Wei Zhao and Norbert C. Cheung

Department of Electrical Engineering, Hong Kong Polytechnic University, Hunghom, Kowloon, Hong Kong SAR, China (e-mail: eencheun@polyu.edu.hk).

Abstract: In this paper, a passivity-based control (PBC) algorithm with disturbance estimation is proposed to obtain precise position control of a Linear Switched Reluctance Motor (LSRM) driving system. Following the modeling analysis of the driving system, a full-order controlled model is first developed. On the basis of the state error equation, the proposed robust PBC algorithm is derived from the view of energy dissipation and the global stability of the whole servo system is insured by the proposed algorithm in turn. Through the disturbance estimation, it can also reject the effect from external disturbances and make the servo system achieve precise position tracking. Simulations and experimental implementations carried out on the proposed LSRM driving system demonstrate that the proposed control algorithm is effective for the LSRM position tracking system.

1. INTRODUCTION

Linear Switched Reluctance Motors (LSRMs) have drawn much research attention over the past decade, due to its low cost, simple structure, ruggedness and reliability in harsh environments, and its potential for numerous industrial applications. Compared to the method of rotary motors with transformation components for producing linear motion, LSRM has many advantages, such as quick response, high sensitivity and excellent tracking capability. Moreover, the structure of a LSRM can reduce the space requirement for its installation. On the other hand, comparing to direct-drive Permanent Magnet Linear Synchronous Motor (PMLSM), a LSRM has a simpler and more rugged structure, and a lower system cost. These advantages make LSRM an alternative choice for direct-drive applications. However, the main limitation of LSRM applications comes from its control and high ripples problem since the mathematical models of LSRM is highly dependent on their complicated magnetic characteristics which are difficult to be modelled, simulated and controlled.

Several control methods and schemes have been proposed to overcome these problems. The most common method is to use lookup table for the nonlinear torque/force compensation (Taylor (1991) and Gan (2003)). These control schemes are based on the fact that current response is much quicker than mechanical response, and the Switched Reluctance Motors (SRMs) are treated as a combination of fast and slow components. However, at the same time, the current dynamics are neglected for the controller design of outer loop and the errors are produced as a result of the differences between dynamic and static states. Other literatures proposed nonlinear control methods for the SRM. Two feedback linearization controllers are designed for position and speed tracking (Ilic'-Spong (1987) and Panda (1996)), where two full-order nonlinear models are applied. Two adaptive controllers are presented to combat the nonlinear characteristics by the online estimation by Bortoff (1998) and Milman (1999). Followed these literature, three passivity-based controllers (Espinosa-Pérez (2004), Yang (2004) and Chan (2005)) are employed for SRMs and variable reluctance finger grippers, respectively. In the above control methods, various nonlinearities in the motion system are taken into account. However, all these control methods assumed that the system model is precise or the unknown parameters can be accurately estimated by online identification and unknown disturbances are not taken into account.

In this paper, we proposed a nonlinear control algorithm with disturbance estimation for the LSRM servo system based on the natural energy dissipation (Maschke (2000) and Ortega (2001)). Firstly, the full-order LSRM model is derived from the model analysis of the driving system. In virtue of the system model, a PBC algorithm with disturbance estimation is designed. The resultant control algorithm guarantees global stability and rejection ability against external disturbances. Detailed simulations and experimental results illustrate that the proposed control algorithm is effective to perform precise position control on the LSRM driving system.

2. CONSTRUCTION AND MODELING OF LSRM

2.1 Configuration of LSRM

The proposed LSRM is a three-phase motor and the design schematic is shown in Fig. 1. Three phase coils with the same dimensions are installed on the moving platform. The body of

the moving platform is manufactured with aluminium, so that the total weight of the moving platform is low and the magnetic paths are decoupled. The moving platform is mounted on two slider blocks which are tightly fixed on the bottom of the LSRM. This rugged mechanical structure can effectively buffer vibration during the operations. The stator track and the core of the windings are laminated with 0.5mm silicon-steel plates.

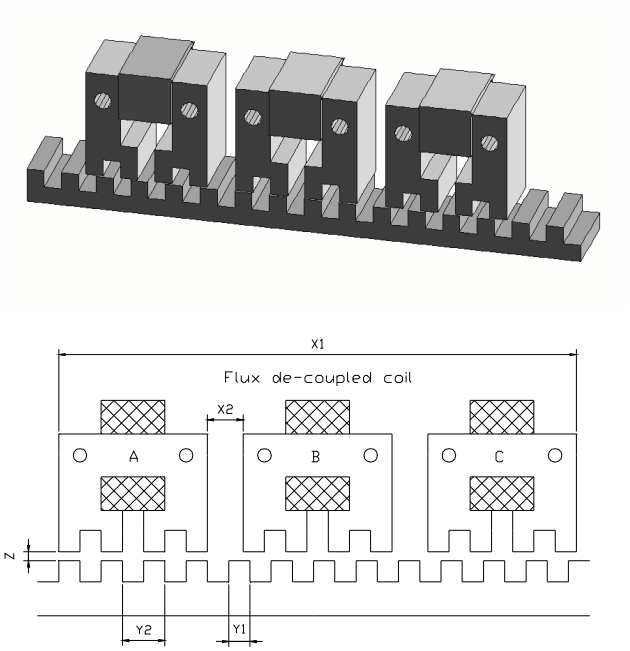

Fig. 1 Schematic of the LSRM.

2.2 Modeling of LSRM

The fundamental equations of LSRM are included as the voltage balance equation (1) and the mechanical movement equation (2). Because the flux linkage is a function of the current and position, the voltage equation can be further expanded as (3).

$$V_j = r_j i_j + \frac{d\lambda_j}{dt}, j = a,b,c \tag{1}$$

$$M\frac{dv}{dt} = F_e - Bv - F_l \tag{2}$$

$$V_j = r_j i_j + L_j \frac{di_j}{dt} + \frac{dL_l}{dx} i_j v, j = a,b,c \tag{3}$$

where V_j and i_j denote the terminals voltage and the current; λ_j L_j and r_j denote the flux linkage, the phase inductance and the winding resistance. x and v denote position and velocity; M and B denote the mass and friction constant. F_e denotes the generated electromagnetic force and F_l denotes the external load force.

The phase force produced can be represented as (4) in the linear region. It can be seen that the force is a nonlinear function of the position and phase current. The total force produced is the sum of each phase force as (5).

$$F_j(x,i_j) = \frac{1}{2}\frac{dL_j}{dx} i_j^2, j = a,b,c\,. \tag{4}$$

$$F_e = \sum_{j=a}^{c} F_j\,. \tag{5}$$

3. PBC DESIGN FOR LSRM

3.1 Commutation of LSRM

As in SRMs, commutation is very important for effectively operating LSRMs. This is mainly derived from the fact that the direction of each phase force generated in a LSRM is dependent upon its current position as shown in (4). In a LSRM, the desired force performance is carried out by the synchronous commutation with its current position. Also, the commutation results in the force ripples. By using multi-phase excitation scheme, therefore, force sharing strategy (Ilic'-Spong (1987) and Gan (2003)) can be applied to obtain smooth force output.

For any given position, there are two sets corresponding to the phases of positive force produced and the phases of negative force produced as

$$\Theta^+ = \{j : \frac{\partial L_j(x)}{\partial x} \geq 0\} \text{ and } \Theta^- = \{j : \frac{\partial L_j(x)}{\partial x} < 0\}\,.$$

Then the force sharing strategy can be performed by a force distribution function (FDF)

$$FDF(x,F_d) = F_d\begin{bmatrix} w_a(x) & w_b(x) & w_c(x)\end{bmatrix} \tag{6}$$

where F_d denotes the desired total force and w_j denotes the weight of force for phase j. A FDF should satisfy the principles in (7) and (8) as follows

$$\begin{cases} F_d \geq 0, w_j(x) > 0\ \forall j \in \Theta^+ \text{ and } w_j(x) = 0\ \forall j \in \Theta^- \\ F_d < 0, w_j(x) > 0\ \forall j \in \Theta^- \text{ and } w_j(x) = 0\ \forall j \in \Theta^+ \end{cases} \tag{7}$$

$$\sum_{j=a}^{c} w_j(x) = 1\,. \tag{8}$$

Hence, a FDF can be used to calculate the desired phase force according to the position and the total desired force. The selection of weight depends on the different force sharing strategies, but any force sharing strategy should satisfy that the sum of each weight should be 1, which means that the sum of each phase force agrees with the desired force. For the drive system, the control signals are the phase voltages, which can be calculated from the desired phase force and the flux linkage model.

3.2 Controller design

In this system, the state vector is $X=[x \quad v \quad i_a \quad i_b \quad i_c]^T$. According to equation (1) to (3), the full-order model can be arranged as follows

$$D\dot{X}=[J(X)-R]X+gu+\xi \tag{9}$$

where g denotes input matrix, u denotes control vector and ξ denotes disturbances. $J(X)$ is a skew-symmetric matrix, satisfied $J^T(X)=-J(X)$. R is a semi-positive definite symmetric matrix and corresponds to the energy dissipating of the model. D is a positive definite matrix.

$$J(X)=\begin{bmatrix} 0 & 1 & 0 & 0 & 0 \\ -1 & 0 & \frac{1}{2}\frac{dL_a}{dx}i_a & \frac{1}{2}\frac{dL_b}{dx}i_b & \frac{1}{2}\frac{dL_c}{dx}i_c \\ 0 & -\frac{1}{2}\frac{dL_a}{dx}i_a & 0 & 0 & 0 \\ 0 & -\frac{1}{2}\frac{dL_b}{dx}i_b & 0 & 0 & 0 \\ 0 & -\frac{1}{2}\frac{dL_c}{dx}i_c & 0 & 0 & 0 \end{bmatrix},$$

$$R=\begin{bmatrix} 0 & 0 & 0 & 0 & 0 \\ 0 & B & 0 & 0 & 0 \\ 0 & 0 & r_a & 0 & 0 \\ 0 & 0 & 0 & r_b & 0 \\ 0 & 0 & 0 & 0 & r_c \end{bmatrix}, \quad g=\begin{bmatrix} 0 & 0 & 0 & 0 & 0 \\ 0 & 0 & 0 & 0 & 0 \\ 0 & 0 & 1 & 0 & 0 \\ 0 & 0 & 0 & 1 & 0 \\ 0 & 0 & 0 & 0 & 1 \end{bmatrix},$$

$$D=\begin{bmatrix} 1 & 0 & 0 & 0 & 0 \\ 0 & M & 0 & 0 & 0 \\ 0 & 0 & L_a & 0 & 0 \\ 0 & 0 & 0 & L_b & 0 \\ 0 & 0 & 0 & 0 & L_c \end{bmatrix}, \; u=\begin{bmatrix} 0 \\ 0 \\ u_a \\ u_b \\ u_c \end{bmatrix} \text{ and}$$

$$\xi^T=[0 \quad x-F_l \quad -\frac{1}{2}\frac{dL_a}{dx}i_a v \quad -\frac{1}{2}\frac{dL_b}{dx}i_b v \quad -\frac{1}{2}\frac{dL_c}{dx}i_c v].$$

The state error is defined as

$$e=X-X_d \tag{10}$$

where X_d denotes the desired system performance.

By substituting the state error into (9), the error model of the system is represented as

$$D\dot{e}+[R-J(X)]e=-D\dot{X}_d-[R-J(X)]X_d+gu+\xi=\Phi_1. \tag{11}$$

Define the energy function of state error as

$$H(e)=\frac{1}{2}e^T De. \tag{12}$$

The derivative of the energy function is described as (13) which can be expanded as (14) and reformatted as (15).

$$\dot{H}(e)=-e^T D\dot{e}+\frac{1}{2}e^T\dot{D}e. \tag{13}$$

$$\dot{H}(e)=-e^T[R-J(X)]e+e^T\Phi_1+\frac{1}{2}e^T\dot{D}e. \tag{14}$$

$$\dot{H}(e)=-e^T Re+e^T(\Phi_1+\frac{1}{2}\dot{D}e). \tag{15}$$

Suppose the derivative of the energy function is restricted in a non-positive region, the error energy function would be eventually dissipated to the minimum and the state variable would reach the equilibrium. It can be achieved by using (16) to design the control algorithm.

$$\Phi_1+\frac{1}{2}\dot{D}e=-Ke \tag{16}$$

where $K=diag\{k_1,k_2,k_3,k_3,k_3\}$ is a positive definite diagonal matrix. As shown in (17), the dissipation of the error energy function is inherently determined by the positive definite diagonal matrix $R+K$.

$$\dot{H}(e)=-e^T(R+K)e. \tag{17}$$

3.3 Disturbance rejection

From theoretical viewpoint, the control algorithm is elegant. However, there always exist unknown disturbances in actual applications, such as external load and static friction, etc. These disturbances would degrade system performances and be expected to be compensated. To obtain high precision, this paper proposes an estimating approach to reject the external load disturbances.

In general, external loads can be considered as constant or slowly varying. Define the estimation error of load as

$$\Delta F_l=\hat{F}_l-F_l \tag{18}$$

where $\hat{F}_l$ is the estimated load. In terms of the estimated load, the disturbance vector can be represented as (19).

$$\xi=\hat{\xi}+\Delta\xi \tag{19}$$

where

$\hat{\xi}=[0 \quad x-\hat{F}_l \quad -\frac{1}{2}\frac{dL_a}{dx}i_a v \quad -\frac{1}{2}\frac{dL_b}{dx}i_b v \quad -\frac{1}{2}\frac{dL_c}{dx}i_c v]^T$ and $\Delta\xi=[0 \quad \Delta F_l \quad 0 \quad 0 \quad 0]^T$.

In this case, the error model of the system can be rearranged as follows

$$\begin{aligned} & D\dot{e}+[R-J(X)]e \\ &= -D\dot{X}_d-[R-J(X)]X_d+gu+\hat{\xi}+\Delta\xi \\ &= \Phi_2+\Delta\xi \end{aligned} \quad (20)$$

where $\Phi_2=-D\dot{X}_d-[R-J(X)]X_d+gu+\hat{\xi}$.

To estimate the load, redefine the error energy function as

$$H(e)=\frac{1}{2}e^T De+\frac{1}{2}\frac{1}{k_4}\Delta F_l^2, k_4>0. \quad (21)$$

The derivative of the energy function with respect to time is

$$\dot{H}(e)=-e^T Re+e^T(\Phi_2+\frac{1}{2}\dot{D}e)+\Delta F_l(\frac{1}{k_4}\Delta\dot{F}_l+e_2) \quad (22)$$

where e_2 denotes the second element of e.

As the differential form of (18), it can be simplified as (23) in that the actual load is assumed as constant and its derivative is equal to zero.

$$\Delta\dot{F}_l=\dot{\hat{F}}_l-\dot{F}_l=\dot{\hat{F}}_l. \quad (23)$$

Therefore, the external load can be estimated by using (24). Moreover, the third term on the right hand side of (22) is cancelled. The estimation speed is dependent upon k_4.

$$\hat{F}_l=-k_4\int e_2 dt. \quad (24)$$

Following this way, the error energy function would also be dissipated to zero by choosing control law with (25).

$$\Phi_2+\frac{1}{2}\dot{D}e=-Ke. \quad (25)$$

The difference between (16) and (25) is that the external load in (25) is estimated online while that in (16) is assumed accurately known. Hence, the unknown disturbances can be estimated and rejected by using the proposed algorithm.

Therefore, the control law can be obtained from (26) by expanding (25) with the estimated load from (24). It is clear that the control variables and the state variables are linked together by the desired state variable. The state variables can be measured from sensors; hence, the control variables can be obtained by solving the desired state variables.

From the first equation of (26), the desired speed can be calculated by using the reference position. The desired phase currents can be calculated by using the desired speed. Each phase voltage is obtained by substituting the measured state variable and the desired state variables into the rest equations.

$$\begin{cases} v_d=\dfrac{dx_d}{dt}+k_1(x_d-x) \\ \dfrac{1}{2}\sum_{j=a}^{c}\dfrac{dL_j}{dx}i_j i_{jd}=M\dfrac{dv_d}{dt}+Bv_d+x_d-x+\hat{F}_l+k_2(v_d-v) \\ V_a=L_a\dfrac{di_{ad}}{dt}+r_a i_{ad}+\dfrac{1}{2}\dfrac{dL_a}{dx}i_a v_d+\dfrac{1}{2}\dfrac{dL_a}{dx}i_{ad}v+k_3(i_{ad}-i_a) \\ V_b=L_b\dfrac{di_{bd}}{dt}+r_b i_{bd}+\dfrac{1}{2}\dfrac{dL_b}{dx}i_b v_d+\dfrac{1}{2}\dfrac{dL_b}{dx}i_{bd}v+k_3(i_{bd}-i_b) \\ V_c=L_c\dfrac{di_{cd}}{dt}+r_c i_{cd}+\dfrac{1}{2}\dfrac{dL_c}{dx}i_c v_d+\dfrac{1}{2}\dfrac{dL_c}{dx}i_{cd}v+k_3(i_{cd}-i_c) \end{cases} \quad (26)$$

The second equation describes the mechanical behaviours of the servo system. The left hand side of this equation denotes the total desired force. Each desired phase force is dependent upon the applied FDF. And the reference phase currents are determined by using each desired phase force. In this paper, the applied FDF is described as Table 1.

Table 1 Force distribution function (FDF) scheme

Position	+ force command	- force command
0mm-2mm	$F_B=F_d$	$F_C=0.5(2-x)F_d$, $F_A=0.5xF_d$
2mm-4mm	$F_B=0.5(4-x)F_d$, $F_C=0.5(x-2)F_d$	$F_A=F_d$
4mm-6mm	$F_C=F_d$	$F_A=0.5(6-x)F_d$, $F_B=0.5(x-4)F_d$
6mm-8mm	$F_C=0.5(8-x)F_d$, $F_A=0.5(x-6)F_d$	$F_B=F_d$
8mm-10mm	$F_A=F_d$	$F_B=0.5(10-x)F_d$, $F_C=0.5(x-8)F_d$
10mm-12mm	$F_A=0.5(12-x)F_d$, $F_B=0.5(x-10)F_d$	$F_C=F_d$

The FDF can adopt either the static or dynamic form. With the neglect of the transient of the force, the second equation of (26) can be simplified as an algebraic equation, in which the actual phase currents are treated as the desired ones. While the transient of force are taken into account, the actual phase currents are usually different from their desired phase currents and need to be collected by current sensors. As a trade-off, the FDF can be adopted the static form to simplify the controller design and ensure an acceptable performance.

Also, it can be seen that the current controller in the last three equations is a proportional controller plus compensation. But the compensation is difficult to be accurately implemented because the system parameters are often hard to be precisely obtained. For the current controller, hence, it is reasonable to reduce the dependence on the system parameters and improve the response speed by increasing the proportional coefficient.

4. SIMULATION RESULTS

In this section, the performance of the proposed algorithm is illustrated by simulation results, which are achieved by the MATLAB software package. LSRM parameters employed in the simulations are listed in Appendix A.

Figure 2 shows the simulation results under a sudden load at the sixth second. As shown in figure 2 (a), response profile of the proposed PBC with disturbance estimation can track the reference accurately after a short transient even under an external disturbance. In ideal case, the general PBC can track the reference well but the response loses its accuracy when a disturbance is loaded. Figure 2 (b) shows the control signals, actual external load and estimated load. From the bottom graph of figure 2 (b), it is clear that the steady value of the estimated load agrees with the actual load well.

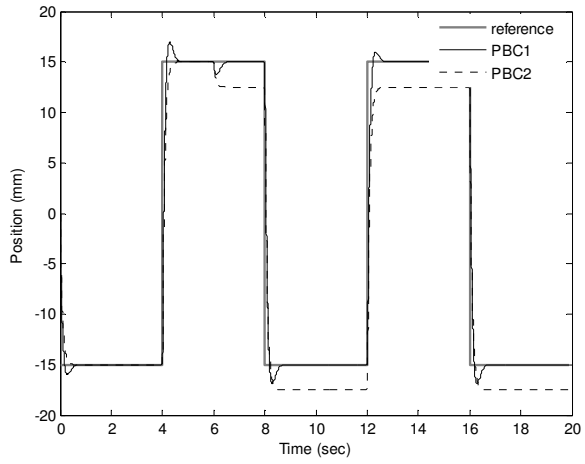

(a)

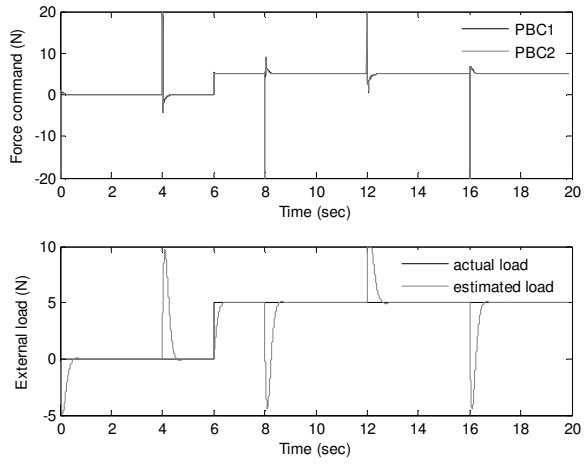

(b)

Fig. 2 Simulation results in the case of a sudden load at the sixth second. (a) Response profiles of the proposed PBC with disturbance estimation (PBC1 as the solid curve) and the general PBC (PBC2 as the dashed curve). (b) The top figure shows the control signals and the bottom figure shows the actual external load and the estimated load.

5. EXPERIMENTAL IMPLEMENTATION RESULTS

As shown in figure 3, the drive system consists of a host PC for controlling, a driver, position and current sensors, and the LSRM. The host PC is used to design the control algorithm, download the target code into a dSPACE DS1104 card, which is plugged into a PCI bus of the host PC, and provide an interface to adjust the system parameters online. The control algorithm is developed under the environment of MATLAB/SIMULINK. All of the control functions are implemented and state variables are sampled by using the DS1104 card. The driver consists of three asymmetric bridge MOSFET inverters with a DC voltage supply. A linear optical encoder with 0.5um resolution is mounted on the moving platform of the LSRM to provide position feedback information.

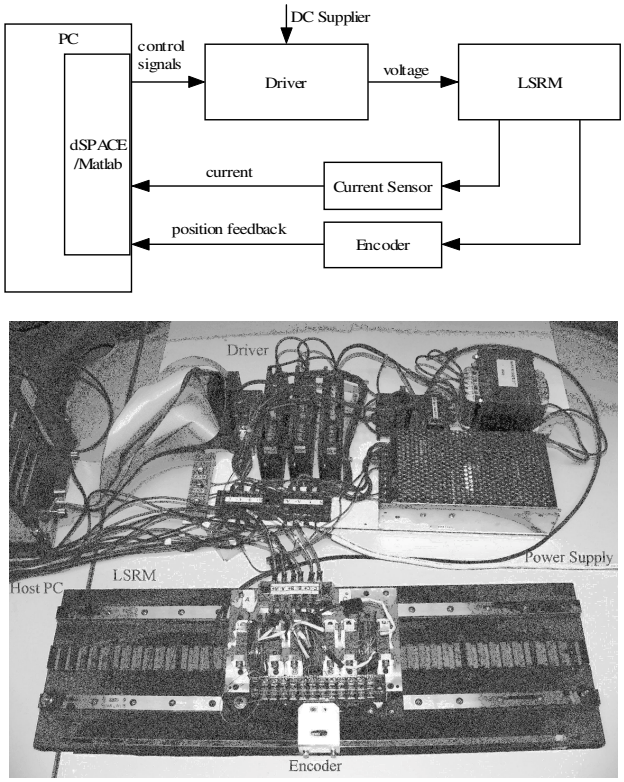

Fig. 3 The experimental setup of the LSRM drive system.

Similar to above simulations, corresponding experiments are carried out on the LSRM drive system to investigate the performance of the proposed algorithm for rejecting external unknown load disturbances.

Figure 4 shows experimental results of the position tracking under static friction and unknown external load. Both of the control algorithms can stably track the reference position. However, it can be clearly observed the precision of the two control algorithms is different under the disturbances. There is no steady error for the proposed control algorithm as the solid curve (PBC1) in figure 4 (a), while some errors exist in the output under the general control algorithm as the dashed curve (PBC2) in figure 4 (a). The corresponded control signals and the estimated load are shown in figure 4 (b). The experimental results match those of simulations well.

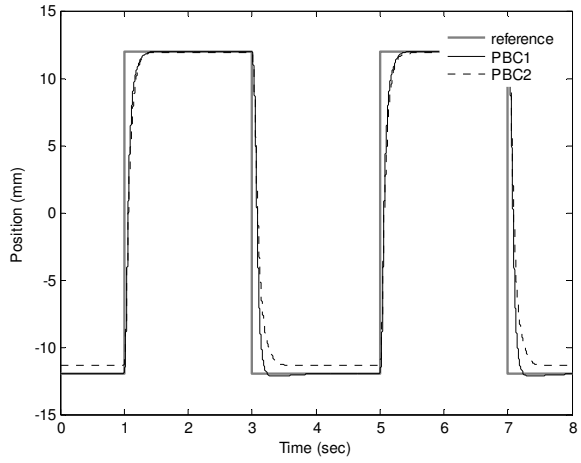

(a)

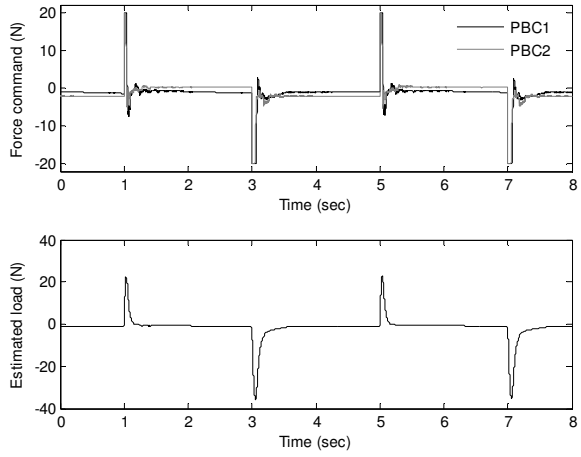

(b)

Fig. 4 Experimental results with an unknown external load. (a) Response profiles of the proposed PBC with disturbance estimation (PBC1 as the solid curve) and the general PBC (PBC2 as the dashed curve). (b) The top figure shows the control signals and the bottom figure shows the estimated load.

6. CONCLUSIONS

A PBC algorithm with disturbance estimation is proposed for precise position tracking of LSRM driving system. From energy dissipation, the proposed algorithm guarantees the global stability of the whole driving system. By using the technique of disturbance estimation, the proposed control algorithm has the ability to reject static frictions and external load disturbances.

To confirm the effectiveness of the proposed algorithm, simulations and experimental implementations are carried out on the proposed driving system. It can be found that the experimental results match those of the simulations well. These results show that the proposed algorithm has an excellent trajectory tracking performance and is robust in the high precision position tracking of the LSRM.

ACKNOWLEDGMENT

The authors would like to thank the University Grants Council for the funding support of this research work through project code: PolyU 5224/04E.

REFERENCES

Taylor, D.G. (1991). An experimental study on composite control of switched reluctance motors. *IEEE Contr. Sys. Magazine*, **11(2),** 31-36.

Gan, W.C., N.C. Cheung and L. Qiu (2003). Position control of linear switched reluctance motors for high precision applications. *IEEE Trans. Ind. Applicat.*, **39(5),** 1350-1362.

Ilic'-Spong, M., R. Marino, S.M. Peresada and D.G. Taylor (1987). Feedback linearizing control of switched reluctance motors. *IEEE Trans. Automat. Contr.*, **AC-32,** 371-379.

Panda, S.K. and P.K. Dash (1996). Application of nonlinear control to switched reluctance motors: a feedback linearization approach. *IEE Pro.-Electr. Power Appl.*, **143,** 371-379.

Bortoff, S.A., R.R. Kohan and R. Milman (1998). Adaptive control of variable reluctance motors: a spline function approach. *IEEE Trans. Ind. Electron.*, **45,** 433-444.

Milman, R. and S.A. Bortoff (1999). Observer-based adaptive control of a variable reluctance motor: experimental results. *IEEE Trans. Contr. System Tech.*, **7,** 613-621.

Espinosa-Pérez, G., P. Maya-Ortiz, M. Velasco-Villa and H. Sira-Ramíez (2004). Passivity-based control of switched reluctance motors with nonlinear magnetic circuits. *IEEE Trans. Contr. System Tech.*, **12,** 439-448.

Yang, J.M., X. Jin, J. Wu, N.C. Cheung and K.K. Chan (2004). Passivity-based control incorporating trajectory planning for a variable-reluctance finger gripper. *Proc. Instn Mech. Engrs Part I: J. Systems and Control Engineering*, **218,** 99-109.

Chan, K.K., J.M. Yang and N.C. Cheung (2005). Passivity-based control for flux regulation in a variable reluctance finger gripper. *IEE Pro.-Electr. Power Appl.*, **152,** 686-694.

Maschke, B., R. Ortega and A.J. van ser Scharf (2000). Energy-based Lyapunov functions for forced Hamiltonian systems with dissipation. *IEEE Trans. Automat. Contr.*, **45,** 1498-1502.

Ortega, R., A.J. van ser Scharf, I. Mareels and B. Maschke (2001). Putting energy back in control. *IEEE Contr. Sys. Magazine*, **21,** 18-33.

Appendix A. Parameters of the LSRM

Pole width (y_1)	6mm
Pole pitch (y_2)	12mm
Motor length (x_1)	146mm
Phase separation (x_2)	10mm
Air gap width (z)	0.5mm
Phase resistance	1.5Ω
Aligned inductance	10.2mH
Unaligned inductance	7.8mH
Mass of the moving platform (M)	1.8Kg